

DOI: 10.1002/cssc.201300527



Synthesis of Pt–Cu Nanodendrites through Controlled Reduction Kinetics for Enhanced Methanol Electro-Oxidation

Eric Taylor,^[a] Shutang Chen,^[a] Jing Tao,^[b] Lijun Wu,^[b] Yimei Zhu,^[b] and Jingyi Chen^{*[a]}

Metal nanoparticles with dendritic structures are of particular interest because of their different chemical and physical properties compared to polyhedral nanoparticles. Owing to the large surface area and the rich step-surface atoms, dendritic nanostructures have been demonstrated to be more catalytically active than conventional polyhedra for many reactions, such as O₂ reduction,^[1–3] methanol oxidation,^[4,5] formic acid oxidation,^[6] ethanol oxidation,^[7] and other small molecule reactions.^[8,9] A small number of synthetic strategies have previously been developed for the synthesis of bimetallic nanodendrites, for example a seed-mediated method has been reported for synthesizing a dense array of Pt branches on a Pd core, with a truncated-octahedral shape, by directly reducing the precursor on the core or by attaching the reduced clusters to the core.^[1,10] Seeded growth has also been demonstrated in nonaqueous systems by using oleylamine to reduce Pt-monolayer particles on Pd cores.^[2] In addition, the seeded-growth method has been confined within silica templates to generate Pt-on-Au nanodendrites.^[3] Another approach is a block-copolymer-mediated method, in which Pd and Pt precursors were simultaneously reduced by using ascorbic acid, yielding Pt-on-Pd nanodendrites.^[4] In this case, the triblock copolymer assisted the phase segregation to form a core-shell dendritic structure. Although most strategies have focused on core-shell nanodendrites, synthetic methods for alloyed nanodendrites are largely lacking. Recently, alloyed Pt–Ni nanodendrites were obtained through a solvothermal approach, which facilitated the effective diffusion to form alloys in a autoclave device; however, control over the composition remains a challenge.^[9] Herein, we report a co-reduction method for the synthesis of alloyed nanodendrites that involves a kinetically controlled reduction, in which ethylene glycol couples to oxidative etchants before fast reduction with ascorbic acid. This approach is initially demonstrated by using a Pt–Cu system.

Pt–Cu nanostructures have received considerable interest because of their bifunctionality that synergistically improves their catalytic activity towards electrochemical reactions associated with fuel-cell applications, for example methanol oxidation.^[11] For this reaction, Pt is the best-known catalyst for the oxidation of methanol to CO-related intermediate species, whereas Cu is active for CO oxidation with water. Together, Pt–Cu alloys activate both methanol and water in the electro-oxidation of methanol, which can effectively remove adsorbed intermediates from the catalyst surface.^[12,13] A number of Pt–Cu nanostructures that further enhance the electrocatalytic activity of methanol have previously been reported, including nanocubes,^[14,15] nanocages,^[16,17] nanorods,^[18,19] and concave structures.^[20] Because the catalytic activity improves with an increased number of active sites, nanodendrites, having a large surface area and high density of step-surface atoms, are promising catalyst candidates for heterogeneous catalysis. In this work, Pt–Cu nanodendrites were synthesized for the first time by using a kinetically controlled co-reduction method. The composition and complexity of the nanodendrites were readily manipulated by varying the reaction time of the rate-limiting step. These dendritic nanostructures show superior catalytic activity in the electro-oxidation of methanol.

As an initial demonstration, Pt₃Cu nanodendrites were synthesized by using a two-step co-reduction of Pt and Cu precursors in a 1:1 molar ratio. The first step was modified from the previously reported polyol synthesis of branched Pt nanoparticles by introducing Cu precursors,^[21,22] and the second step was to accelerate the reduction process by using a stronger reducing agent (i.e., ascorbic acid). At the initial stage, the precursors were reduced by using ethylene glycol in the air, with a small amount of additives (i.e., FeCl₃ and HCl). These additives and O₂ in the air served as oxidative etchants, which could react with the reduced species to return it to the oxidized form. The color of the reaction mixture turned from orange–yellow to green–yellow within 1 h, and the mixture retained the green–yellow color for a long period of time (i.e., 24 h) before the addition of ascorbic acid, indicating that the reduction of the precursor was very slow.^[21] As soon as the ascorbic acid was added to the reaction, the solution turned from green–yellow to dark-brown within 15 min, yielding the nanodendrites with a diameter of approximately 30 nm (Figure 1 A). The lattice constant (*a*) of the nanodendrites was obtained through analysis of the X-ray diffraction (XRD) pattern to be 0.384 nm (Figure 1 B). Assuming the linear-mixing rule, the composition of the nanodendrites was estimated as Pt₃Cu, based on Vegard's Law (*a*_{Pt} = 0.392 nm and *a*_{Cu} = 0.361 nm).^[23]

[a] E. Taylor, Dr. S. Chen, Prof. J. Chen
Department of Chemistry and Biochemistry
University of Arkansas, Fayetteville, AR 72701 (USA)
Fax: (+1) 479-575-6203
E-mail: chenj@uark.edu

[b] Dr. J. Tao, Dr. L. Wu, Dr. Y. Zhu
Condensed Matter Physics and Materials Science Department
Brookhaven National Laboratory, Upton, NY 11973 (USA)

 Supporting Information for this article is available on the WWW under <http://dx.doi.org/10.1002/cssc.201300527>.

 Part of a Special Issue on "Shaping Nanostructures for Applications in Energy Conversion and Storage". To view the complete issue, visit: <http://onlinelibrary.wiley.com/doi/10.1002/cssc.v6.10/issuetoc>

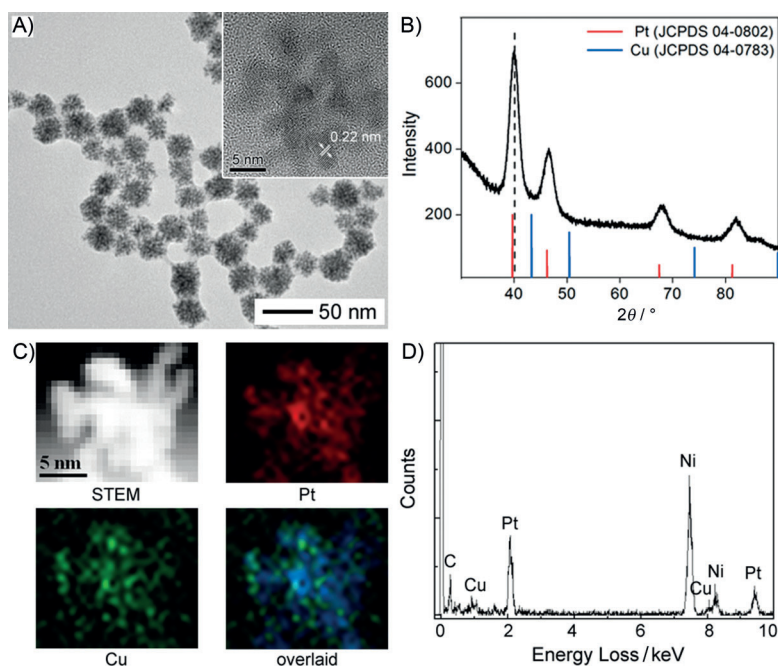


Figure 1. A) Transmission electron microscopy (TEM) image and B) XRD pattern of Pt₃Cu nanodendrites synthesized by using a co-reduction method, which involved a two-step procedure with an initial slow reduction that utilized ethylene glycol for 24 h, followed by a fast 15 min reduction step that used ascorbic acid. Inset: High-resolution TEM (HRTEM) image of an individual nanodendrite. C) Energy-dispersive X-ray (EDX) elemental mapping and D) EDX elemental analysis of an individual nanodendrite on a Ni grid.

HRTEM analysis indicated that each branch of the nanodendrites had a width of approximately 3 nm and grew along the $\langle 111 \rangle$ direction of the Pt₃Cu face-centered cubic structure (see Figure S1 in the Supporting Information). The mixed-alloy atomic arrangement of the nanodendrites was further confirmed by using EDX mapping analysis (Figure 1C). The high-angle annular dark-field scanning transmission electron microscopy (HAADF-STEM) image, in which each pixel was overlaid with the results from elemental mapping, was simultaneously acquired with the EDX analysis. The zoomed-out HAADF-STEM image has been included in Figure S2 to display the mapping area. The results showed that elemental Pt and Cu were evenly distributed across the dendritic nanoparticle. Elemental analysis revealed a 3:1 atomic ratio of Pt/Cu for individual nanodendrites (Figure 1D). The increase in the stoichiometric ratio (Pt/Cu) from 1:1 (feeding ratio of precursors) to 3:1 (atomic ratio of the product) can be explained because 1) the reduction of Cu only occurs in second step and 2) the galvanic replacement of Cu with Pt^{II} leads to the dissolution of Cu back to Cu^{II}.

The UV/Vis study was performed to monitor the disappearance of the precursors during the synthesis, which could validate these hypotheses (Figure S3). The broad peak at approximately 850 nm could be assigned to Cu-glycol complexes,^[24,25] with the absorption coefficient estimated as $32.2 \pm 0.8 \text{ L mol}^{-1} \text{ cm}^{-1}$. There was no change in the peak intensity after reduction for 24 h in ethyl glycol, indicating that no reduction of the Cu precursor occurred in this step. Although the peak intensity of supernatant was close to zero after ascorbic acid reduction, we could not rule out the possibility that

Cu^{II} was absorbed on the nanoparticle surface or coordinated with polyvinylpyrrolidone (PVP) in the precipitates. Nevertheless, these results suggested that more Pt was reduced compared to Cu in the first step, and thus more Pt was reduced throughout the entire synthesis.

The morphology of the product was essentially controlled through the reduction kinetics of the slow reduction step by using ethylene glycol as a reducing agent, with a small amount of oxidative etchants. Figure 2 shows the morphology and composition of the nanostructures obtained from the two-step co-reduction, which resulted from various reaction times of the initial step and the same reduction time (i.e., 15 min) for the second step. The size and complexity of the dendritic structures increased with extended reaction times. The re-

sultant products were ultra-small dendrites (diameter ≈ 5 nm, Figure 2A), medium dendrites (diameter ≈ 20 nm, Figure 2B), and large dendrites (diameter ≈ 30 nm, Figure 2C), which were obtained after 2, 6, and 12 h reduction in the first step, respectively. HRTEM analysis (inset of Figure 2A) showed that the growth direction was along the $\langle 111 \rangle$ axis for each branch (≈ 3 nm wide) of the ultra-small dendrites, in agreement with that observed for the large dendrites. XRD analysis indicated that the composition of each sample varied from Pt₅₀Cu₅₀ (PtCu) to Pt₆₅Cu₃₅ and Pt₇₅Cu₂₅ (Pt₃Cu) for reaction times 2, 6 or 12, and 24 h, respectively (Figure 2D). The ratio of Pt/Cu increased with extended reduction time in the first step, that is, prior to the addition of ascorbic acid, suggesting that the reduction of Pt predominantly occurred in the initial reduction with ethylene glycol. During this kinetically controlled process, the single-crystalline seeds of Pt preferentially grew along the $\langle 111 \rangle$ axis.^[21,22,26,27] To induce over-growth on the $\{111\}$ facets, the presence of the H⁺ and Cl⁻ appeared to be crucial. As a control experiment, the reaction without the addition of FeCl₃ and HCl was performed, which led to the formation of spherical Pt₃Cu nanoparticles (Figure S4). Extension of the reaction time led to an increase in the size and the number of the seeds in the solution, resulting in an increased percentage of Pt in each nanodendrite. As nanoparticles overgrew along the same axis, the lattice spacing of their activated sites was matched. Therefore, the increased number of seeds in the prolonged reaction led to the coalescence of the single-crystal seeds and, subsequently, the formation of larger nanodendrites.^[28]

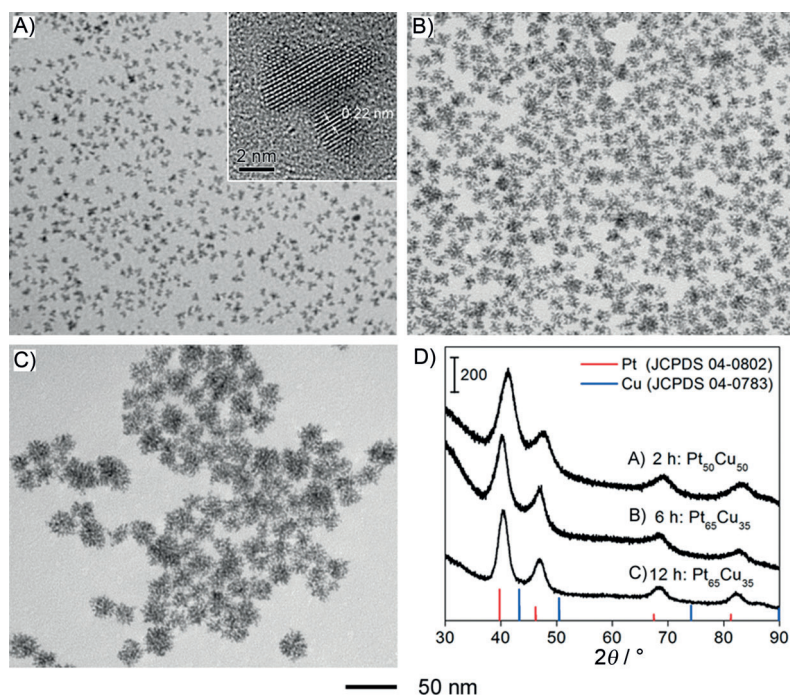


Figure 2. TEM images of the Pt–Cu nanostructures that resulted from A) 2 h, B) 6 h, C) and 12 h reaction time of the initial step, before the addition of ascorbic acid. D) XRD patterns of the corresponding samples shown (A–C).

The dendritic nanostructures provided a large surface area and a large number of active sites for electrocatalysis. The electrochemically active surface area (ECSA) was determined by integrating the charge involved in hydrogen desorption, within the potential range of 0.05–0.4 V versus a reversible hydrogen electrode (RHE),^[29] after correction for the double-layer capacitive contribution. Assuming a polycrystalline surface, the charge associated with the desorption of a hydrogen monolayer is $210 \mu\text{C cm}^{-2}$.^[30,31] The ECSA was estimated to be 112.5, 58.5, and $109.5 \text{ m}^2 \text{ g}_{\text{Pt}}^{-1}$ for Pt₃Cu nanodendrites, Pt₃Cu spherical nanoparticles, and the commercial carbon-supported Pt catalyst (Pt/C, 20 wt% Pt), respectively (Figure 3A). Before loading onto the carbon support, the ECSA of the Pt₃Cu nanodendrites was roughly the same as that of the commercial Pt/C material, and the ECSA was approximately two times larger than that of the spherical Pt₃Cu nanoparticles. The increase in the ECSA could be attributed to the dendritic morphology, which prevented the agglomeration of the nanoparticles during the electrode preparation process.

The catalytic activity of the Pt₃Cu nanodendrites was examined towards the electro-oxidation of methanol. Figure 3B shows the cyclic voltammetry (CV) profiles of each sample in a 1 M CH₃OH/0.1 M HClO₄ solution at a scan rate of 50 mV s^{-1} . The oxidative current density of the forward sweep (I_f) was recorded to be 0.50, 0.18, and 0.17 mA cm^{-2} for Pt₃Cu nanodendrites, Pt₃Cu nanoparticles, and Pt/C, respectively. The I_f value for the nanodendrites was 2.8 times of that of the Pt₃Cu nanoparticles and Pt/C, indicating a high efficiency for methanol oxidation. The current density of the backward sweep (I_b) was also recorded, and the ratio of I_f/I_b for the Pt₃Cu nanodendrites was 1.32, which was comparable to that of the Pt₃Cu nanopar-

ticles ($I_f/I_b=1.69$), but higher than that of the Pt/C catalyst ($I_f/I_b=0.87$). This result implied that the Pt–Cu alloy oxidized methanol more effectively and with less poisoning-intermediates adsorbed on the surface than Pt/C.^[12] These findings were further confirmed by using chronoamperometry (CA), which was performed at 0.9 V for 1200 s (Figure 3C). The current density of the Pt₃Cu nanodendrites was higher than that of both the Pt₃Cu nanoparticles and Pt/C throughout the measurement. The high activity of the Pt₃Cu nanodendrites could be attributed to the unique dendrite structure and the bi-functionality of Pt and Cu for promoting methanol oxidation.

The stability of the Pt₃Cu nanodendrites was further investigated by using the potential cycling treatment performed in Ar-saturated 0.1 M HClO₄ solution, at a scan rate of 50 mV s^{-1} for 250 cycles at room temperature (Figure 3D). The ECSA of the Pt₃Cu nanodendrites was calculated as 88, 90, 82, and $55 \text{ m}^2 \text{ g}_{\text{Pt}}^{-1}$ after 2, 20, 100, and 250 cycles, respectively. The decrease in the ECSA after 250 cycles was possibly caused by the dissolution of the catalyst from the electrode. The performance

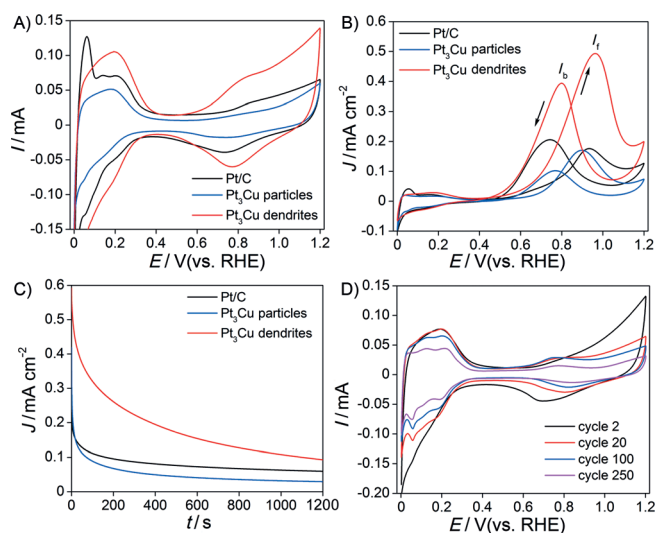


Figure 3. A) CV profiles (scan rate = 50 mV s^{-1}) of the Pt₃Cu nanodendrites, Pt₃Cu nanoparticles, and Pt/C material in 0.1 M HClO₄ solution. B) CV and C) CA of methanol oxidation on Pt₃Cu nanodendrites, Pt₃Cu nanoparticles, and Pt/C in a solution containing 1 M methanol and 0.1 M HClO₄ at a scan rate of 50 mV s^{-1} . The CA curves were obtained at 0.9 V versus RHE. D) CV profiles of the Pt₃Cu nanodendrites in 0.1 M HClO₄ solution at a scan rate of 50 mV s^{-1} .

of the catalyst was further characterized for methanol oxidation after 250 cycles, and compared to the performance after 20 cycles (Figure S5). The I_f value was recorded to be 0.5 mA cm^{-2} after 20 cycles and 0.24 mA cm^{-2} after 250 cycles, whereas I_f/I_b was calculated as 1.32 and 2.87 after 20 and 250 cycles, respectively. After 250 cycles, the nanodendrites were removed from the electrode surface and their morphology and composition were analyzed by using TEM and EDX mapping (Figure S6). The dendritic shape of the nanoparticles remained unchanged as the atomic ratio of Pt/Cu increased from 3:1 to 5:1 owing to the dissolution of Cu under the acidic conditions.^[16,32]

In summary, Pt–Cu nanodendrites were synthesized by using a two-step co-reduction method, which involved a kinetically controlled slow reduction step and, subsequently, a fast reduction process. The dendritic nanostructures were the result of overgrowth on the {111} facets and the coalescence of small dendritic seeds. The size and composition of the Pt–Cu nanodendrites increased as the reaction time during the slow reduction step was increased. This method provided a straightforward synthesis for the production of Pt-containing alloyed nanodendrites. The Pt₃Cu nanodendrites exhibited large ECSA, high current density, and better CO-resistance for methanol oxidation compared to Pt₃Cu nanoparticles and the commercial Pt/C catalyst.

Experimental Section

Synthesis of Pt–Cu nanodendrites

In a typical synthesis, ethylene glycol (4 mL) was added to a 25 mL three-necked round-bottom flask equipped with a water-cooling condenser and heated to 110 °C. After 1 h, 6 mM HCl in ethylene glycol (50 μL) and 200 mM FeCl₃ in ethylene glycol (100 μL) were simultaneously injected into the flask. After 1 min, 32 mM H₂PtCl₆·6H₂O (2 mL, 33 mg, 64 μmol), PVP (2 mL, $M_n=55000$, 0.045 g), and 32 mM CuCl₂ (8.5 mg, 63 μmol) in ethylene glycol (2 mL) were simultaneously injected into the flask. The reaction mixture was then maintained at 110 °C for a period of time varying from 2 to 24 h. The color of the reaction changed from golden-yellow to green–yellow, indicating the reduction of the Pt precursor. After this initial period of slow reduction, 500 mM ascorbic acid (0.5 mL) was added to the reaction mixture to accelerate the reduction as a second step. Within 15 min, the color of the reaction mixture changed from green–yellow to dark-brown, indicating the formation of nanoparticles. The product was then precipitated out by using acetone and centrifugation (five times), followed by washing with ethanol (twice). The sample was dried under vacuum overnight.

Instrumentation

TEM images were captured by using a JEOL 1011 microscope with an accelerating voltage of 100 kV. HRTEM images, HAADF–STEM images, and EDX maps were obtained by using a JEOL-ARM 200F microscope with an acceleration voltage of 200 kV. XRD patterns were acquired by using a Rigaku MiniFlex X-ray diffractometer equipped with a CuK α radiation source operated at 30 kV and 15 mA. The concentration of Pt was determined by using a GBC 932 atomic absorption spectrometer.

Electrochemical measurements

The electrocatalytic activity of the Pt–Cu nanodendrites and commercial Pt/C (20 wt% Pt) was characterized by using CV and CA on a CHI760 electrochemical workstation at room temperature. The measurements were performed by using a three-electrode cell with a Ag/AgCl/1.0 M KCl reference electrode (standard electrode potential, $E^0 = -0.294 \text{ V}$ vs. RHE) and a Pt wire as the counter electrode. A glassy carbon disk (0.070 cm²) was polished to a mirror-finish before each experiment, and was used as the substrate for the working electrode. The catalyst suspension was prepared by mixing a $0.8 \text{ mg}_{\text{Pt}} \text{ mL}^{-1}$ nanoparticle suspension with 0.05 wt% Nafion (1:1 v/v), which was then subjected to sonication for 5 min. An aliquot of the suspension (5 μL) was pipetted onto the glassy carbon substrate, yielding a Pt loading of 2 μg (or 28 $\mu\text{g cm}^{-2}$). The working electrode was dried at room temperature. The ECSA was determined from the CV profiles obtained at a scan rate of 50 mV s^{-1} in 0.1 M HClO₄ solution. The methanol oxidation was performed in a solution containing 1.0 M CH₃OH and 0.1 M HClO₄ at a scan rate of 50 mV s^{-1} . CA was recorded at 0.9 V versus RHE in a solution containing 1.0 M CH₃OH and 0.1 M HClO₄. The electrochemical dealloying process was performed at a scan rate of 50 mV s^{-1} , within the potential range from 0–1.2 V versus RHE in 0.1 M HClO₄ solution. After a certain number of cycles, the CV profile was recorded at a scan rate of 50 mV s^{-1} .

Acknowledgements

This work was supported in part by the Ralph E. Powe Jr. Faculty Enhancement Award and start-up funds from the University of Arkansas awarded to J.C. The work at Brookhaven National Laboratory was supported by the US Department of Energy (Basic Energy Sciences) and by the Materials Science and Engineering Division under Contract No. DE-AC02-98CH10886.

Keywords: alloys • copper • methanol oxidation • nanoparticles • platinum

- [1] B. Lim, M. Jiang, P. H. C. Camargo, E. C. Cho, J. Tao, X. Lu, Y. Zhu, Y. Xia, *Science* **2009**, *324*, 1302–1305.
- [2] Z. Peng, H. Yang, *J. Am. Chem. Soc.* **2009**, *131*, 7542–7543.
- [3] K. M. Yeo, S. Choi, R. M. Anisur, J. Kim, I. S. Lee, *Angew. Chem.* **2011**, *123*, 771–774; *Angew. Chem. Int. Ed.* **2011**, *50*, 745–748.
- [4] L. Wang, Y. Nemoto, Y. Yamauchi, *J. Am. Chem. Soc.* **2011**, *133*, 9674–9677.
- [5] Z.-H. Lin, M.-H. Lin, H.-T. Chang, *Chem. Eur. J.* **2009**, *15*, 4656–4662.
- [6] N. Ortiz, S. E. Skrabalak, *Angew. Chem.* **2012**, *124*, 11927–11931; *Angew. Chem. Int. Ed.* **2012**, *51*, 11757–11761.
- [7] Q. Gao, M.-R. Gao, J.-W. Liu, M.-Y. Chen, C.-H. Cui, H.-H. Li, S.-H. Yu, *Nanoscale* **2013**, *5*, 3202–3207.
- [8] A. Mohanty, N. Garg, R. Jin, *Angew. Chem.* **2010**, *122*, 5082–5086; *Angew. Chem. Int. Ed.* **2010**, *49*, 4962–4966.
- [9] W. Wang, D. Wang, X. Liu, Q. Peng, Y. Li, *Chem. Commun.* **2013**, *49*, 2903–2905.
- [10] B. Lim, M. Jiang, T. Yu, P. C. Camargo, Y. Xia, *Nano Res.* **2010**, *3*, 69–80.
- [11] A. Rabis, P. Rodriguez, T. J. Schmidt, *ACS Catal.* **2012**, *2*, 864–890.
- [12] J. Rossmesl, P. Ferrin, G. A. Tritsarlis, A. U. Nilekar, S. Koh, S. E. Bae, S. R. Brankovic, P. Strasser, M. Mavrikakis, *Energy Environ. Sci.* **2012**, *5*, 8335–8342.
- [13] G. A. Tritsarlis, J. Rossmesl, *J. Phys. Chem. C* **2012**, *116*, 11980–11986.
- [14] D. Xu, Z. Liu, H. Yang, Q. Liu, J. Zhang, J. Fang, S. Zou, K. Sun, *Angew. Chem.* **2009**, *121*, 4281–4285; *Angew. Chem. Int. Ed.* **2009**, *48*, 4217–4221.

- [15] A.-X. Yin, X.-Q. Min, W. Zhu, W.-C. Liu, Y.-W. Zhang, C.-H. Yan, *Chem. Eur. J.* **2012**, *18*, 777–782.
- [16] B. Y. Xia, H. B. Wu, X. Wang, X. W. Lou, *J. Am. Chem. Soc.* **2012**, *134*, 13934–13937.
- [17] F. Nosheen, Z.-c. Zhang, J. Zhuang, X. Wang, *Nanoscale* **2013**, *5*, 3660–3663.
- [18] Q. Liu, Z. Yan, N. L. Henderson, J. C. Bauer, D. W. Goodman, J. D. Batteas, R. E. Schaak, *J. Am. Chem. Soc.* **2009**, *131*, 5720–5721.
- [19] S. Chen, S. V. Jenkins, J. Tao, Y. Zhu, J. Chen, *J. Phys. Chem. C* **2013**, *117*, 8924–8932.
- [20] X. Liu, W. Wang, H. Li, L. Li, G. Zhou, R. Yu, D. Wang, Y. Li, *Sci. Rep.* **2013**, *3*, 1404.
- [21] J. Chen, T. Herricks, M. Geissler, Y. Xia, *J. Am. Chem. Soc.* **2004**, *126*, 10854–10855.
- [22] J. Chen, T. Herricks, Y. Xia, *Angew. Chem.* **2005**, *117*, 2645–2648; *Angew. Chem. Int. Ed.* **2005**, *44*, 2589–2592.
- [23] W. B. Pearson, *A Handbook of Lattice Spacings and Structures of Metals and Alloys*, Pergamon Press, New York, **1958**.
- [24] H. B. Jonassen, R. E. Reeves, L. Segal, *J. Am. Chem. Soc.* **1955**, *77*, 2667–2670.
- [25] J. W. Mehl, *J. Biol. Chem.* **1945**, *157*, 173–180.
- [26] J. Chen, Y. Xiong, Y. Yin, Y. Xia, *Small* **2006**, *2*, 1340–1343.
- [27] L. Ma, C. Wang, M. Gong, L. Liao, R. Long, J. Wang, D. Wu, W. Zhong, M. J. Kim, Y. Chen, Y. Xie, Y. Xiong, *ACS Nano* **2012**, *6*, 9797–9806.
- [28] H.-G. Liao, L. Cui, S. Whitlam, H. Zheng, *Science* **2012**, *336*, 1011–1014.
- [29] T. Biegler, D. A. J. Rand, R. Woods, *J. Electroanal. Chem. Interfacial Electrochem.* **1971**, *29*, 269–277.
- [30] N. M. Marković, B. N. Grgur, P. N. Ross, *J. Phys. Chem. B* **1997**, *101*, 5405–5413.
- [31] W. Wielstich, A. Lamm, H. A. Gasteiger, *Handbook of Fuel Cells: Fundamentals, Technology, Applications*, Vol. 2, Wiley, West Sussex, **2003**.
- [32] S. Koh, P. Strasser, *J. Am. Chem. Soc.* **2007**, *129*, 12624–12625.

Received: May 31, 2013

Revised: July 25, 2013

Published online on September 17, 2013